

Flow penetration into the canopy of the submerged vegetation: definitions and quantitative estimates

N. Nikora & V. Nikora

School of Engineering, University of Aberdeen, Aberdeen, Scotland, UK

ABSTRACT: The focus of this study is on the ranges of flow submergence and vegetation density which well exceed the ranges already studied by other researchers. The penetration distance δ_e of large-scale turbulence into vegetation canopies has been assessed using vertical distributions of the normal and shear turbulent stresses. Although the estimates of δ_e by the suggested methods are interconnected, their values may differ reflecting different aspects of flow-vegetation interactions. The estimates based on the shear stresses $\overline{u'w'}$ are most closely correlated with those from the profiles of the variance of the longitudinal velocity $\overline{u'u'}$ and thus can be used when two-component velocity measurements are not possible. The experimental assessment of the influence of characteristic turbulence scales and energy on flow penetration parameters was made using dimensionless numbers characterizing the interplay between depth-scale, canopy-scale, and wake-scale turbulent eddies. The data suggest that there may be mutually opposing effects leading to unexpected behaviors such as the blockage of depth-scale eddies by enhanced wake-scale turbulence.

Keywords: Flow-vegetation interactions, Penetration depth, Penetration distance

1 INTRODUCTION

Aquatic vegetation in streams is common and plays significant roles in physical and ecological processes. It affects magnitudes and spatial distributions of mean velocities and turbulence properties and thus often controls transport of water (i.e., channel conveyance capacity), sediments, nutrients and contaminants. In recent years, a number of extensive studies exploring turbulence structure within a vegetation canopy and in the flow region above have been conducted advancing the understanding of flow-vegetation interactions, e.g., Nepf & Vivoni (2000), Wilson et al. (2003), Poggi et al. (2004), Järvelä (2005), Sukhodolov & Sukhodolova (2006), Nepf et al. (2007), Velasco et al. (2007), Maltese et al. (2007), Nepf & Ghisalberti (2008), Nezu & Sanjou (2008), Righetti (2008), Okamoto & Nezu (2009), Stoesser et al. (2009). It has been found that a key feature of flow-vegetation interactions is the generation of a shear layer at the border between aquatic vegetation and the overlying water flow. The thickness of this interface region is controlled by the flow and plant characteristics and can be estimated by

the distance of flow penetration into the vegetation canopy. The experimental and theoretical studies suggest that the penetration distance should be considered as an integral measure of the flow-vegetation interactions that may be successfully used in a number of ways. These may include, among others, determination of the effective bed roughness, zero-plane displacement, separation of the canopy into regions of 'vertical' and 'horizontal' exchange of scalar and momentum, and longitudinal dispersion in vegetated channels, Nepf & Vivoni (2000), Nepf et al. (2007). Although the cited studies have significantly advanced the understanding of flow penetration into vegetation canopies, they relate to quite limited ranges of driving parameters (e.g., flow submergence, vegetation morphology and density, plant flexural rigidity) and considerable knowledge gaps remain.

The key objectives of this paper, therefore, include: (1) revision of the existing and consideration of new definitions for flow penetration distance and their estimates and comparisons; and (2) experimental assessment of the effects of characteristic turbulence scales and energy on flow pe-

netration parameters. The focus of our study is on the ranges of flow submergence and vegetation density which well exceed the ranges already studied by other researchers.

2 BACKGROUND

Based on an experimental study of depth-limited vegetated flow, Nepf & Vivoni (2000) proposed that the vegetation canopy may be subdivided into two regions with distinctly different mechanisms of flow forcing, turbulence production, and exchange with surrounding waters. The upper region (“upper canopy”) is largely controlled by the vertical turbulent momentum flux while the lower region (“lower canopy”) is predominantly pressure- or gravity-driven. Turbulence in the upper canopy is generated by the shear layer at the canopy top. The mechanism of turbulence production within the lower canopy is different and is mainly due to flow separations in plant wakes. The exchange with surrounding waters within the lower canopy is dominated by longitudinal advection, while in the upper canopy – by vertical turbulent exchange. Following Raupach et al. (1996), Nepf and Vivoni (2000), Ghisalberti & Nepf (2002, 2004), and Nepf et al. (2007) suggested that the penetration distance of the turbulent stress into the canopy is controlled by the vortices generated at the canopy top due to the Kelvin-Helmholtz (KH) instability. These vortices are known as ‘mixing-layer vortices’ as opposed to the ‘boundary-layer vortices’. As a measure of penetration, Nepf and Vivoni (2000) proposed the “penetration depth”, h_p , that is defined as the distance from the bed to the point where turbulent stress decays to 10% of its maximum value (Figure 1). Another useful measure, suggested in Nepf et al. (2007), is the distance δ_e from the top of the canopy to the level where turbulent stress diminishes to 10% of its peak value, i.e., $\delta_e = h_c - h_p$ (see definitions in Figure 1). Wilson et al. (2003) introduced a length scale of vortex penetration, similar to δ_e , that they defined as the thickness of the active momentum exchange layer. Several follow up studies have also highlighted that the penetration depth h_p (or distance δ_e) is an integral measure of momentum and scalar transfer into vegetation, e.g., Velasco et al. (2007), Nezu & Sanjou (2008), Okamoto & Nezu (2009). Quantitative estimates of h_p and δ_e in these studies are based on a “10% technique” applied to the $\overline{u'w'}$ profiles as originally suggested by Nepf and Vivoni (2000).

Although Nepf and Vivoni’s (2000) $\overline{u'w'}$ -based technique is physically appealing there are other possible options. They may include determination of the penetration distance (or depth) using verti-

cal distributions of other components of the Reynolds stress tensor or their combinations (e.g., normal stresses and the total turbulent energy). In addition, the penetration distance (or depth) can also be assessed using the zero-plane displacement d as was suggested in Nepf and Vivoni (2000). We consider the penetration distance δ_e more appropriate than h_p or d , as it directly measures the penetration of large eddies into vegetation canopies (Figure 1) and does not require the existence of the logarithmic layer which is a prerequisite for d .

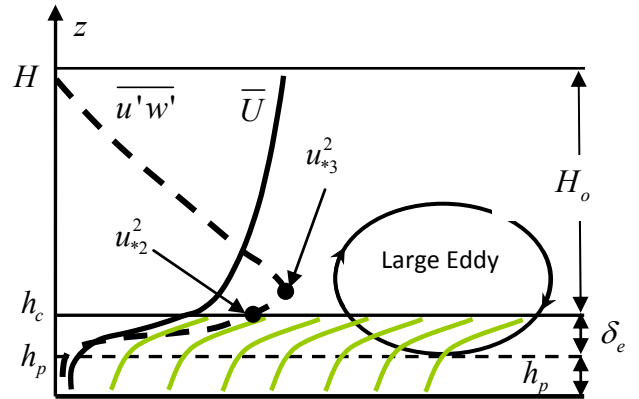


Figure 1. Definition sketch: H is water depth; h_c is deflected canopy height; $H_o = H - h_c$ is the depth of over-flow; mean velocity \overline{U} and turbulent stress $\overline{u'w'}$ profiles are shown by solid and dashed lines, respectively; δ_e is the penetration distance of the large eddies into the canopy; h_p is the penetration depth; solid circles show u_{*2}^2 and u_{*3}^2 definitions.

In this paper we first explore alternative ways for defining δ_e and how they relate to the $\overline{u'w'}$ -based estimates. Then, we assess the effects of the turbulence scales and energy on flow penetration distance, following a general relation:

$$\delta_e = f(L_{BL}, K_{BL}, L_{ML}, K_{ML}, L_W, K_W, g, \nu) \quad (1)$$

where $L_{BL} \propto H_o = H - h_c$ is the boundary-layer-eddy scale, $L_{ML} \propto h_c$ is the mixing-layer-eddy scale, $L_W \propto w$ is the wake-turbulence-eddy scale (w is stem/leaf width), $K_{BL} \propto u_*^2$, $K_{ML} \propto u_*^2$ and $K_W \propto u_*^2$ are turbulent energies associated with $L_{BL} \propto H_o$, $L_{ML} \propto h_c$, and $L_W \propto w$, respectively (u_* is the shear velocity), g is gravity, and ν is fluid viscosity. Effects of vegetation density, morphology, and rigidity are not explicitly included in (Eq. 1) as their study is outside the scope of this paper. From (Eq. 1) it follows:

$$\frac{\delta_e}{h_c} = f\left(\frac{H-h_c}{h_c}, \frac{u_*^2}{g(H-h_c)}, \frac{u_*^2}{gh_c}, \frac{u_* h_c}{\nu}, \frac{u_* w}{\nu}\right) \quad (2)$$

Effects of arguments of (Eq. 2) on the penetration distance will be explored in section 4 while section 3 will outline experimental data and procedures.

3 EXPERIMENTS AND METHODS

3.1 Experimental set up

Laboratory experiments were carried out in a 12.5 m long and 0.3 m wide rectangular glass-sided tilting flume at the Fluid Mechanics Laboratory of the University of Aberdeen (Figure 2). An adjustable weir located at the discharge tank have been used to minimize backwater effects and extend the section of quasi-uniform flow for a given bed slope. Ten piezometric intakes tapped in the centre line of the flume bed were used to measure water surface slope. The water discharge was measured by an orifice flowmeter installed in the pump discharge pipe. The water depth, H , and deflected canopy height, h_c , were measured at ten evenly-spaced cross-sections using decimal rulers, which were glued to the glass side wall of the flume.

The flume bed was fully covered by artificial flexible garden grass made of polyethylene (Figure 2), with grass areal density of 15000 plants/m². Each plant consisted of 16 stems and had a shape similar to a bush (Figure 3). The height h_v , width w , and thickness t of each stem of 13 randomly selected plants (208 stems in total) were measured using digital Vernier scale with uncertainty 0.01 mm, giving averaged values as $h_v=35.9$ mm, $w=1.1$ mm, and $t=0.2$ mm, respectively. Using the size distributions of stems, the frontal area per unit volume (Figure 3) was estimated at $\Delta z=0.5$ mm intervals as:

$$a_i = \frac{w\Delta z N_{si}}{A_b \Delta z} \approx \frac{w}{\Delta A_b} F(s) \quad (3)$$

where a_i is the total frontal area within i^{th} Δz -interval at a distance $i\Delta z$ from the bed, w is the stem width, ΔA_b is bed area associated with one stem, N_{si} is the number of stems within a representative area A_b at $i\Delta z$, $F(s)$ is cumulative distribution function of stem lengths s . For the near bed part of the plant (lowest 1.5 mm) it was assumed that all stems were joined closely together forming a flexible ‘rod’ of 3 mm in diameter. For our experimental grass, the maximum and average frontal areas per unit volume were 265 m⁻¹ and 212 m⁻¹, respectively. The stem flexural rigidity was determined as $J = EI = 3.36 \times 10^{-8}$ Nm², where E is the modulus of elasticity, and I is the second moment of area.

Five sets of experimental runs were conducted for a range of flume bed slopes from 0.05% to 0.3%. For each bed slope, six experiments with flow rates from 10 l/s to 35 l/s were completed giving in total 30 experimental runs (Table 1). The water depths in the experiments ranged from 11.9 cm to 40 cm, which corresponded to relative

submergence H/h_c from 3.5 to 11.8 and to aspect ratio B/H from 0.8 to 2.5 (B is channel width). For this range of B/H , noticeable secondary currents due to the rectangular flow geometry should be expected above the canopy, Nezu & Nakagawa (1993). Although the secondary currents are an inherent feature of most studies of submerged vegetation (e.g., $B/H=0.9 - 2.4$ in Nepf & Vivoni, 2000, or $B/H=1.7 - 3.9$ in Wilson et. al., 2003), their potential effects remain to be properly assessed. Before that we have to assume, similar to other authors, that the impact of the secondary currents on our findings is not significant.

Table 1. Ranges of experimental parameters.

S_b , %	Q , l/s	H/h_c	$Re=UH/v$ ($\times 10^5$)	$Fr=U/(gH)^{1/2}$
0.05 - 0.30	10 - 35	3.5 - 11.8	0.34 - 1.17	0.1 - 0.4

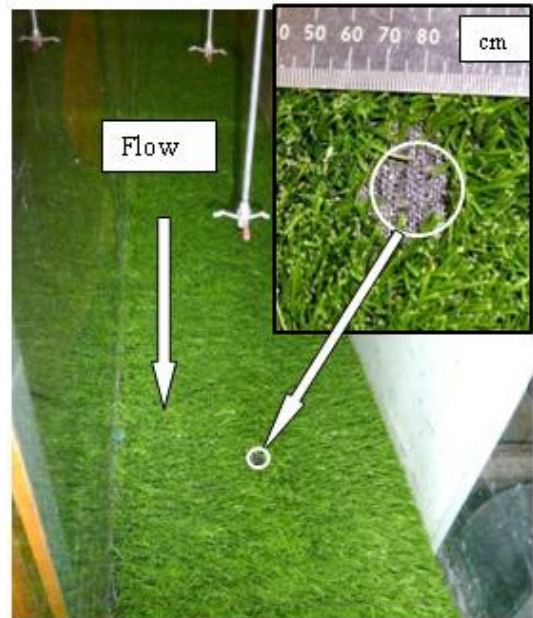


Figure 2. Experimental set-up and a measurement hole within the vegetation canopy.

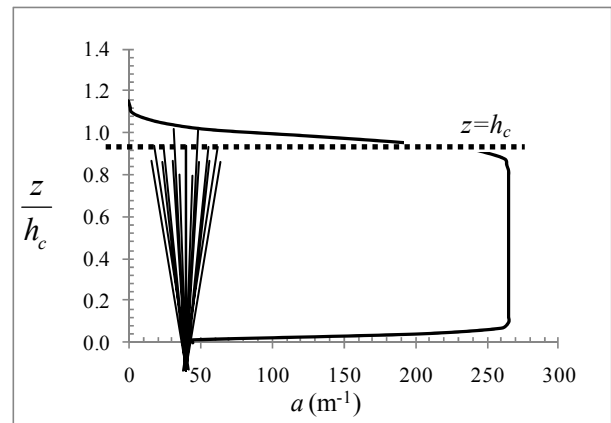


Figure 3. Profile of the vegetation density, a .

To measure velocities, a three-component Nortek down-looking Acoustic Doppler Velocimeter (ADV) was used. The streamwise, lateral and ver-

tical coordinates are denoted as x , y and z , respectively, with $z=0$ at the flume bed. The corresponding time-averaged velocity components and turbulent fluctuations in each direction are defined as U , V , W and u' , v' , w' , respectively. The trial experiments showed that because of the high grass density the removal of 4 plants from a small area of approximately 2 cm by 2 cm was required, to allow measurements within a canopy. The vertical distributions of the time averaged signal-to-noise ratio (SNR) were used to determine the optimal measurement position over the measurement hole. This was identified at the position of the reduced values of SNR. Similar procedure was used by Maltese et al. (2007). Stephan & Gutknecht (2002) used an analogous technique to determine the deflected plant height. To investigate effects of the plants removal on the velocity statistics profiles, the synchronized measurements with 2 ADVs positioned longitudinally along the channel were conducted. First, one ADV was located above the measurement hole and the second ADV was positioned 20 cm upstream. Then, another set of synchronized measurements was taken with the second ADV positioned 20 cm downstream of the hole, keeping the first ADV above the hole. The measurements showed that removal of plants had statistically negligible impact upon the measured velocity statistics, consistent with Ghisalberti & Nepf (2004). All velocity data used in this paper were recorded over the measurement hole located 6 m from the flume entrance and 0.15 m from the flume side walls. The sampling duration of 120 s at a frequency of 25 Hz with a standard measurement volume of 0.25cm^3 were used. Depending on the flow submergence and bed slope, the number of measuring points in a vertical profile varied from 15 to 28, with an average of 24.

3.2 Estimates of the shear velocity

As the shear velocity is one of the key parameters in relationship (Eq. 2), we explored three approaches to define it. In our first approach we estimated the shear velocity as (e.g., Nikora et al. 2001):

$$u_{*1} = \sqrt{gS(H_o + \phi_o h_c)} \quad (4)$$

where $H_o = H - h_c$ is the depth of overflow (Figure 1), $\phi_o = V_f / V_c \approx 0.95 - 0.96$ is vegetation porosity, V_f is the volume of fluid within the total canopy volume V_c . This estimate is equivalent to the conventional definition $u_{*1} = \sqrt{\tau_o / \rho}$, where τ_o is the bed shear stress and ρ is fluid density.

The second and third approaches utilize measured values of the Reynolds stresses $u'w'$ and $v'w'$ as follows:

$$u_{*2,3} = \left[\frac{1}{N_{2,3}} \sum_{i=1}^{N_{2,3}} (\overline{u'w'^2} + \overline{v'w'^2})^{1/2} \right]^{1/2} \quad (5)$$

where $N_2 = 4$, including two Reynolds stress values measured just above h_c and two values – measured below h_c , $N_3 = 2$, including the highest value of the Reynolds stress and the second highest one. The preliminary trials showed that averaging over N_2 and N_3 in (Eq. 5) allowed to significantly reduce effect of variability. The involvement of $\overline{v'w'}$ in computation of the shear velocities (Eq. 5) is to eliminate potential probe misalignment effects.

The estimate u_{*2} corresponds to the Reynolds stress at the top of the canopy while the estimate u_{*3} relates to the maximum of the Reynolds stress that in general can occur slightly above or below the canopy top (Figure 1). The estimates u_{*2} and u_{*3} are more suitable as the scales of the momentum flux compared to u_{*1} , which may be biased by the drag force, e.g., Järvelä (2002), Pokrajac et al., (2006). The data show that u_{*1} is greater, as expected, than u_{*2} and u_{*3} .

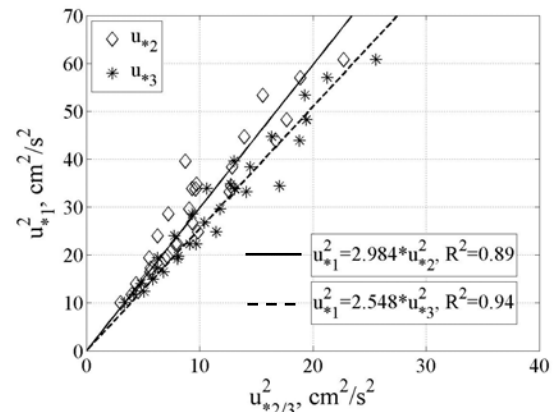


Figure 4. Comparison of squared shear velocity estimates.

The correlation between u_{*1} , u_{*2} and u_{*3} is high (Figure 4) and thus essentially any of them could be used in our considerations. The data and interpretations discussed in section 4 are based on u_{*3} as most physically transparent, and comparable to the previous studies.

3.3 Estimates of the penetration distance

In addition to Nepf and Vivoni's (2000) technique, in our study we explored estimates of δ_e based on the vertical distributions of the total turbulent energy $k = 0.5(\overline{u'u'} + \overline{v'v'} + \overline{w'w'})$ and its components $\overline{u'u'}$, $\overline{v'v'}$, and $\overline{w'w'}$ (which are normal Reynolds stresses). For each case, δ_e was determined at a position corresponding to 10% of the maximum value of a particular stress tensor component, to keep consistency with Nepf and Vivoni's (2000) $\overline{u'w'}$ -based approach. In principle, the estimates of δ_e based on different Rey-

nolds stress components may not coincide as these components may have different penetration mechanisms. We also compare the obtained estimates to the ‘zero-plane displacement’ d (e.g., Nepf and Vivoni, 2000):

$$d = \int_0^{h_c} \frac{d\overline{u'w'}}{dz} dz / \int_0^{h_c} \frac{d\overline{u'u'}}{dz} dz, \quad (6)$$

although, strictly speaking, this estimate is applicable for the constant-shear stress boundary layers only.

4 RESULTS AND DISCUSSIONS

Representative vertical profiles of the normalized longitudinal velocities U and Reynolds stress $\overline{u'w'}$ are shown in Figure 5, where a horizontal solid line denotes the deflected canopy height. Figure 5a shows that the mean flow velocities normalized on u_{*3} collapse well on a single curve within the canopy and a thin region above, up to $z/h_c \approx 1.5-2.0$. However, the measured velocities in the upper flow region demonstrate noticeable divergence, which reflects, most likely, the secondary currents effects. The ratio U/u_* at the canopy top is close to 6.5, on average, varying between 6 and 7. The convincing approximation of the flow velocities in the near-canopy region by a logarithmic law was not successful. This is consistent with previous studies, e.g. Nepf & Vivoni (2000), Velasco et al. (2007), Wilson et al. (2003). The inflection point in velocity profiles is typically slightly below the canopy top, at around $z/h_c \approx 0.8-0.9$. The Reynolds stress $\overline{u'w'}$ normalized on u_{*3} peaks either at the canopy top or slightly above it, being within the range $1.0 \leq z/h_c \leq 1.3$ (Figure b). The normalized turbulence intensities σ_i/u_{*3} show that positions of maximums of σ_u/u_{*3} and σ_v/u_{*3} change from slightly below the canopy top at high bed slopes to slightly above it at low slopes. The intensity σ_w/u_{*3} peaks at around $z/h_c \approx 1.4$ in all cases. Combined together, these features are presented in vertical profiles of k/u_{*3}^2 (Figure. 5c).

The estimates of the penetration distance obtained from the measured profiles of the turbulent shear and normal stresses and turbulent kinetic energy are shown and compared in Figure 6. The estimates of δ_e from the shear stresses $\overline{u'w'}$ are most closely correlated with those from the $\overline{u'u'}$ profiles (Figure 6b). The penetration distances for $\overline{v'v'}$ and especially for $\overline{w'w'}$ are noticeably higher (Figures 6c and 6d). These differences reflect, most likely, specific details of penetration mechanisms for different velocity components, which remain to be investigated. The penetration

distance based on the total turbulent energy (Figure 6a) integrates this information and, thus, may hide the specific mechanisms related to the individual velocity components. The values of d are approximately 25-40% lower than δ_e based on the Reynolds shear stress (Figure 6e). This slightly differs from Nepf & Ghisalberti’s (2008) result who found $d \approx 0.5\delta_e$. This difference is probably due to significantly higher vegetation density in our study. Overall, our analysis demonstrates that although the estimates of δ_e by the selected methods are interconnected they are different and, in principle, may reflect different aspects of flow-vegetation interactions.

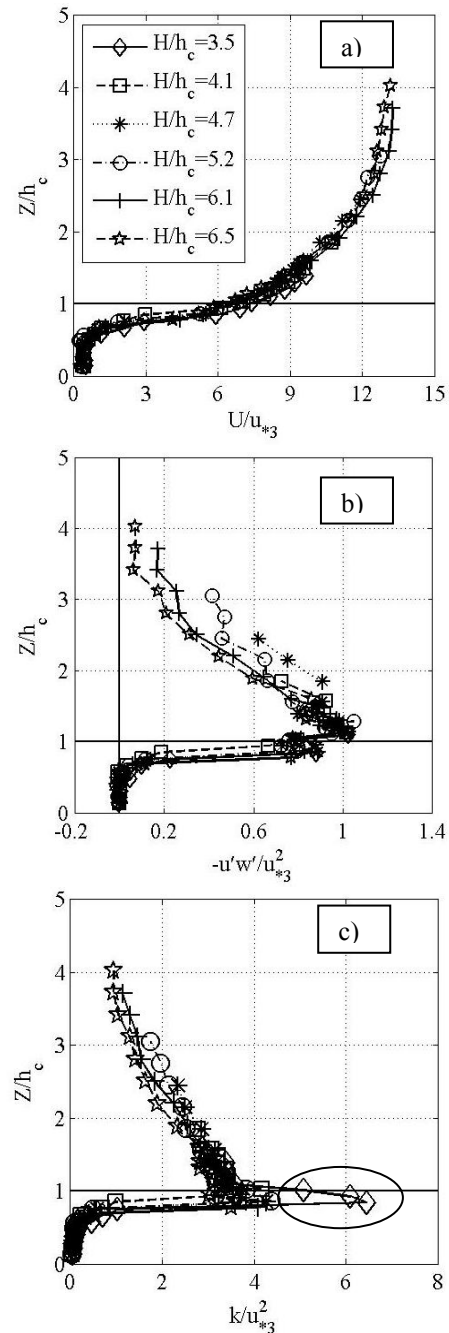


Figure 5. Representative normalized profiles of mean velocity (a), Reynolds stress (b), and total turbulent kinetic energy (c), for $S_b=0.3\%$. Deviations of data points marked by an ellipse in (c) are not clear, but likely due to the measurements’ noise.

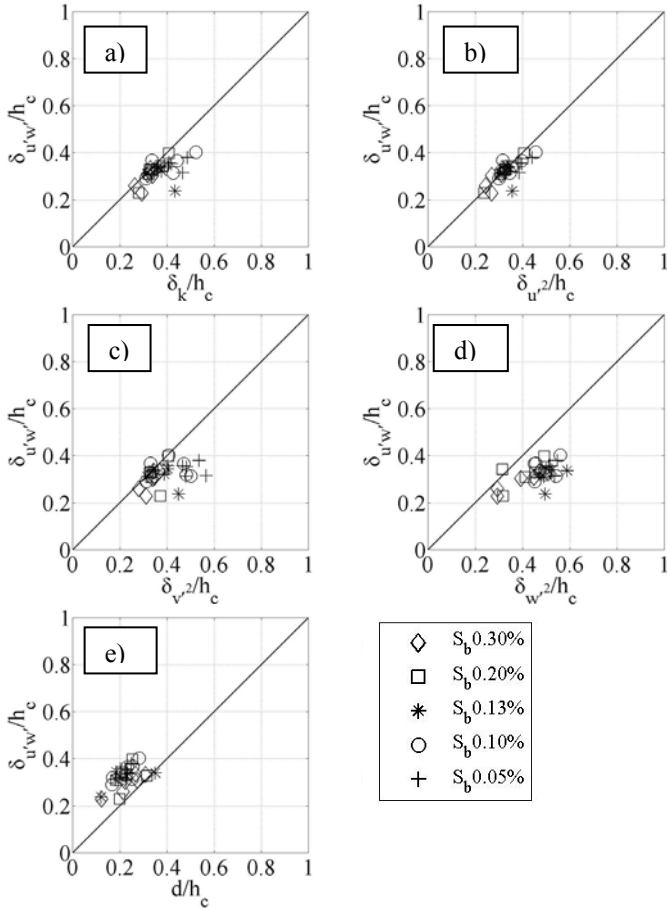


Figure 6. Correlations of relative penetration distance, estimated using Reynolds shear stress profiles, with relative penetration distances estimated using vertical profiles of other components of Reynolds stress tensor and d from Eq. 6.

The dependencies of δ_e on the arguments of relationship (Eq. 2) are shown in Figures 7 to 11. As the estimates of δ_e by different methods are reasonably correlated (Figure 6), the plots in Figures 7 to 11 are based on δ_e from Nepf and Vivoni's (2000) $\overline{u'w'}$ -based approach, to make comparisons with the previous studies easier. The plot $\delta_e/h_c = f((H-h_c)/h_c)$ suggests that the penetration distance increases with increase in submergence until H_o/h_c reaches 5-6 and then it becomes constant or even decreases (Figure 7). This tendency is consistent with Nezu and Sanjou (2008) who demonstrated that δ_e/h_c in their experiments was growing up to a maximum studied submergence, $H/h_c \approx 4$ (i.e., $H_o/h_c \approx 3$). This finding is different, however, from the earlier work of Nepf and Vivoni (2000) whose experiments showed saturation in growth of δ_e/h_c at $H/h_c \approx 2$ (i.e., $H_o/h_c \approx 1$). The noted discrepancy is most likely relates to the significant differences in plant morphologies, densities, and rigidities. The potential effects of the secondary currents should not be dismissed too. The physical mechanism of the δ_e/h_c growth at small H_o/h_c presumably relates to the growth of the large scale eddies with increasing depth, e.g., Nepf & Ghisalberti's (2008). It also should be noted that the ra-

tio H_o/h_c reflects interplay between the depth-scale and canopy-scale eddies that changes with increase in submergence.

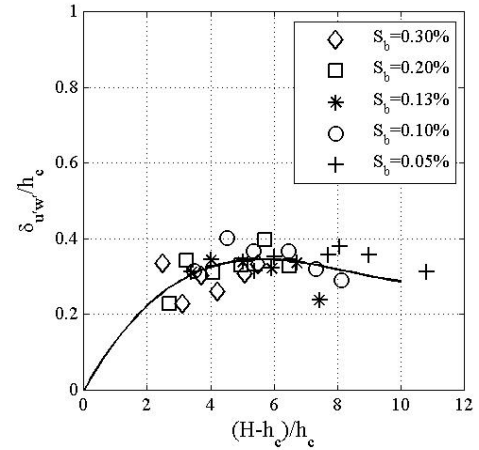


Figure 7. Relation between $\delta_{u'w'}/h_c$ and the relative submergence. Solid line highlights the general trend.

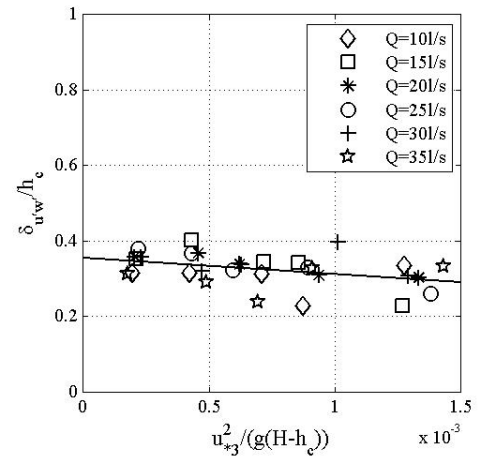


Figure 8. Relation between $\delta_{u'w'}/h_c$ and the 'depth-based' Froude number. Solid line highlights the general trend.

The Froude number $u_*^2/(g(H-h_c))$ in Figure 8 can be interpreted as the depth-scale-eddy energy per unit length-scale, i.e., as an energy density measure of the depth-scale turbulence. The plot $\delta_e/h_c = f(u_*^2/(gH_o))$ shows that the penetration distance gradually decreases with increase in $u_*^2/(gH_o)$, which is unexpected (Figure 8). Indeed, physical considerations suggest that the large-eddy penetration into the canopy should increase with increase in turbulent energy, e.g., Nikora et al. (2002). This discrepancy may be explained by the fact that with increase in the energy of the depth-scale turbulence we also observe increase in the energy of the wake-scale turbulence, effect of which can be quantified using vegetation Reynolds numbers u_*h_c/ν and u_*w/ν . With increase in these numbers, one should expect the enhancement of flow separations from the stems leading to increase in 'turbulent viscosity' that may slow down the penetration of large eddies. Stems' vibrations, noted in the experiments, increase with u_*h_c/ν and may also contribute to

this effect. Plots in Figures 9 and 10 are consistent with this conjecture.

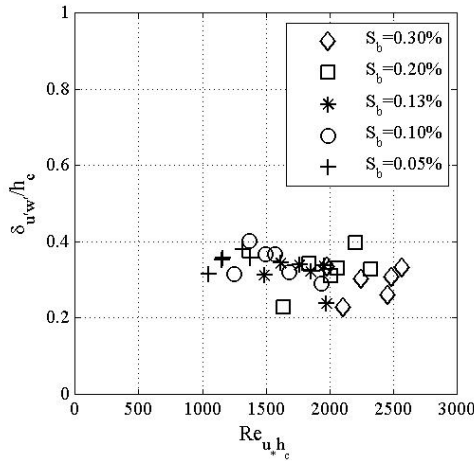


Figure 9. Relation between $\delta_{u'w'}/h_c$ and the ‘canopy’ Reynolds number u_*h_c/ν .

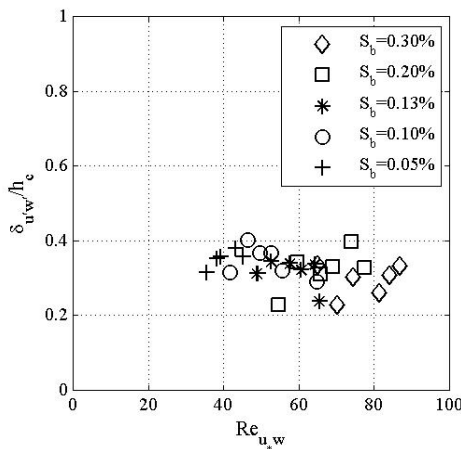


Figure 10. Relation between $\delta_{u'w'}/h_c$ and the ‘stem’ Reynolds number u_*w/ν .

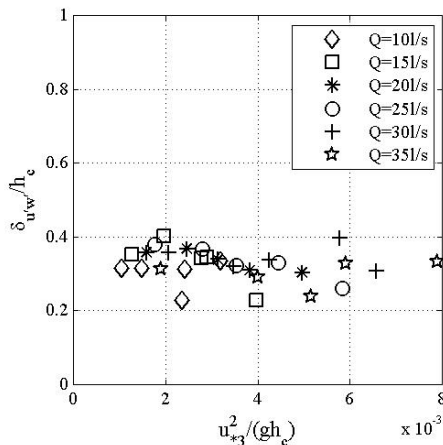


Figure 11. Relation between $\delta_{u'w'}/h_c$ and the ‘canopy-based’ Froude number.

The Froude number $u_*^2/(gh_c)$ in Figure 11 can be interpreted similar to $u_*^2/(gH_o)$, as the canopy-scale-eddy energy per unit length-scale, i.e., as an energy density measure of the canopy-scale turbulence. The plot $\delta_e/h_c = f(u_*^2/(gh_c))$ suggests that this measure was not influential in controlling the penetration distance (Figure 11).

The comparison of our data on the penetration distance with the previous studies (Table 2) is shown in Figure 12. Here, instead of H_o/h_c we use H/h_c as most published data report H/h_c rather than H_o/h_c . The range of the bulk canopy density covered in Figure 12 exceeds 2 orders of magnitude while the range of the flexural rigidity $J=EI$ of studied artificial plants covers 4 orders of magnitude. These wide ranges of the vegetation parameters are reflected in a range of δ_e/h_c from 0.2 to 0.9. Clearly, the vegetation parameters play a significant role in determining the penetration distance and have to be involved into consideration. Our attempt to explain variability of δ_e/h_c in Figure 12 using a recently proposed relationship $\delta_e/h_c = f(C_D ah_c)$, Nepf & Ghisalberti (2008), was not successful highlighting the need for further studies (C_D is the stem drag coefficient).

Table 2. Laboratory data used for comparison in Figure 12.

Experimental study	$J=EI, \text{Nm}^2 \text{a}, \text{m}^{-1}$		Symbol – Figure 12
Dunn et al. (1996)		1.1	□
Wilson et al. (2003)	1.81E-04	1.7	◇
Dunn et al. (1996)		2.5	◁
Okamoto & Nezu (2009)	7.30E-05	3.8	×
Nepf & Vivoni (2000)	1.00E-05	5.5	○
Okamoto & Nezu (2009)	7.30E-05	7.6	+
Wilson et al. (2003)	1.81E-04	22.4	☆
Present study	3.55E-08	265.0	▽

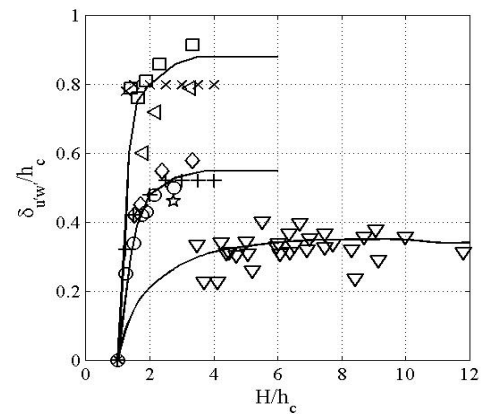


Figure 12. Relation between $\delta_{u'w'}/h_c$ and relative submergence. Solid lines highlight the general trend.

5 CONCLUSIONS

The main findings of the study reported in this paper can be summarized as follows.

1. The penetration distance of large-scale turbulence into vegetation canopies can be effectively assessed using vertical distributions of the normal and shear turbulent stresses. Although the estimates of δ_e by the suggested methods are interconnected, their values may differ reflecting different aspects of flow-vegetation interactions.

The estimates of δ_e from the shear stresses $\overline{u'w'}$ are most closely correlated with those from the $\overline{u'u'}$ profiles and thus can be used when two-component velocity measurements are not possible.

2. The experimental assessment of the influence of characteristic turbulence scales and energy on flow penetration parameters was made using dimensionless numbers characterizing the interplay between the depth-scale, canopy-scale, and wake-scale turbulent eddies. The data suggest that there may be mutually opposing effects leading to unexpected behaviors such as the blockage of depth-scale eddies by enhanced wake-scale turbulence.

3. The focus of our study was on the ranges of flow submergence and vegetation density which well exceed the ranges already studied by other researchers. Thus, our data can help in the identification of the effects missed in previous studies.

ACKNOWLEDGMENTS

The work was partly supported by the Leverhulme Trust, Grant F/00152/Z 'Biophysics of flow-plant interactions in aquatic systems'. The authors are grateful to the following students: G. Clyne, C. Ghirardo, M. Mcconnell, D. Mcmanus, J. Pike, G. Toledano Piriz, M. Witz for helping with laboratory experiments.

REFERENCES

- Dunn, C., Lopez, F., Garcia, M. 1996. Mean flow and turbulence structure induced by vegetation: Experiments. Hydraulic Engineering Series No. 51, UILU-ENG 96-2009, Dept. of Civil Engineering, Univ. of Illinois, Urbana-Champaign, Ill.
- Ghisalberti, M., Nepf, H.M. 2002. Mixing layers and coherent structures in vegetated aquatic flows. *Journal of Geophysical Research*, Vol. 107, No. C2.
- Ghisalberti, M., Nepf, H.M. 2004. The limited growth of vegetated shear layers. *Water Resources Research*, Vol. 40, W07502, 1-12; DOI:10.1029/2003WR002776.
- Järvelä, J. 2002. Flow resistance of flexible and stiff vegetation: a flume study with natural plants. *Journal of Hydrology*, Vol. 269, 44-54.
- Järvelä, J. 2005. Effect of submerged flexible vegetation on flow structure and resistance. *Journal of Hydrology*, Vol. 307, 233-241; DOI:10.1016/j.jhydrol.2004.10.013.
- Maltese, A., Cox, E., Folkard, A.M., Ciraolo, G., La Loggia, G., Lombardo, G. 2007. Laboratory Measurements of Flow and Turbulence in Discontinuous Distributions of Ligulate Seagrass. *Journal Of Hydraulic Engineering*, Vol. 133, No. 7; DOI: 10.1061/(ASCE)0733-9429(2007)133:7(750)
- Nepf, H.M., Vivoni, E.R. 2000. Flow structure in depth-limited, vegetated flow. *Journal of Geophysical Research*, 105(C12), 28,547-28,557.
- Nepf, H.M., Ghisalberti, M., White, B., Murphy, E. 2007. Retention time and dispersion associated with submerged aquatic canopies. *Water Resources Research*, Vol. 43, W04422, 1-10; DOI:10.1029/2006WR005362.
- Nepf, H.M., Ghisalberti, M. 2008. Flow and transport in channels with submerged vegetation. *Acta Geophysica*, 56(3), 753-777; DOI: 10.2478/s11600-008-0017-y.
- Nezu, I., Nakagawa, H. 1993. *Turbulence in Open-Channel Flows*. IAHR-Monograph, Balkema.
- Nezu, I., Sanjou, M. 2008. Turbulence structure and coherent motion in vegetated canopy open-channel flows. *Journal of Hydro-environment Research*, Vol. 2, 62-90; DOI:10.1016/j.jher.2008.05.003.
- Nikora, V.I., Goring, D.G., McEwan, I., Griffiths, G. Spatially-averaged open-channel flow over a rough bed. *Journal of Hydraulic Engineering*, ASCE, 2001, 127(2), 123-133.
- Nikora, V., Koll, K., McLean, S., Dittrich, A., Aberle, J. 2002. Zero-plane displacement for rough-bed open-channel flows. *Proceedings of the International Conference on Fluvial Hydraulics River Flow 2002*, Vol. 1, 83-91.
- Okamoto, T., Nezu, I. 2009. Turbulence structure and "Monami" phenomena in flexible vegetated open-channel flows. *Journal of Hydraulic Research*, 47(6), 798-810; DOI:10.3826/jhr.2009.3536.
- Poggi, D., Porporato, A., Ridolfi, L., Albertson, J. D., Katul, G. G. 2004. The effect of vegetation density on canopy sub-layer turbulence. *Boundary-Layer Meteorology* 111: 565-587.
- Pokrajac, D., Finnigan, J.J., Manees, C., McEwan, I., Nikora, V. 2006. On the definition of the shear velocity in rough bed open channel flows. *Proceedings of the International Conference on Fluvial Hydraulics River Flow 2006*, Vol. 1, 89-98.
- Raupach, M.R., Finnigan, J.J., Brunet, Y. 1996. Coherent eddies and turbulence in vegetation canopies: the mixing layer analogy. *Boundary-Layer Meteorology*, Vol. 78, 351-382.
- Righetti, M. 2008. Flow analysis in a channel with flexible vegetation using double-averaging method. *Acta Geophysica* 56(3): 801-823.; DOI: 10.2478/s11600-008-0032-z.
- Stephan, U., Gutknecht, D. 2002. Hydraulic resistance of submerged flexible vegetation. *Journal of Hydrology*, Vol. 269, 27-43.
- Stoesser, T., Palau Salvador, G., Rodi, W., Diplas, P. 2009. Large Eddy Simulation of turbulent flow through submerged vegetation. *Transport Porous Media*, DOI 10.1007/s11242-009-9371-8.
- Sukhodolov, A., Sukhodolova, T. 2006. Evolution of mixing layers in turbulent flow over submerged vegetation: field experiments and measurement study. *Proceedings of the International Conference on Fluvial Hydraulics River Flow 2006*, Vol. 1, 525-534..
- Velasco, D., Bateman, A., Medina, V. 2007. A new integrated, hydro-mechanical model applied to flexible vegetation in riverbeds. *Journal of Hydraulic Research*, 00(00), 1-19.
- Wilson, C.A.M.E., Stoesser, T., Bates, P.D., Batemann Pinzen, A. 2003. Open channel flow through different forms of submerged flexible vegetation. *Journal of Hydraulic Engineering*, 129(11), 847-853.